Time Scales of Spontaneous Imbibition into Porous Material: From Classic Models to Papers Applications

Pierre-Yves Bloch,[a,*] Konrad Olejnik,[b] Jean-Francis Bloch,[c] Alexandre Bloch,[c] Jules Hammond,[d] and Daniel Brissaud [a]

Flow and spontaneous imbibition phenomena in porous media are important for various industrial applications, including printing and medical lateral flow assays. Their quantitative characterization is important to better understand and select the appropriate raw materials. However, standard methods often require time-consuming tests, and/or expensive equipment. Different time scales must be considered, limiting the range of possible characterization tools. A novel experimental approach based on image analysis for characterizing spontaneous imbibition processes is presented. Hence, ultra-fast diffusion may be quantitatively characterized. Models are issued from the literature to consider physical phenomena at small (milliseconds) and medium range (seconds) of time scales. The obtained experimental data fit with theoretical results, providing valuable insights into the understanding of fluid flow behavior at different time scales. Furthermore, the identification of some physical properties for either the fluid, or the substrate, based on the theoretical models are possible, as the contact angle, which remains to be otherwise challenging. This study contributes to bridging the gap between spontaneous imbibition and capillary phenomena at different time scales, their modeling, and a characterization of material and/or fluid properties paving the way for enhanced understanding and control of fluid behavior in porous media. Different papers are considered to illustrate the method.

DOI: 10.15376/biores.19.1.345-365

Keywords: Fluids; Spontaneous imbibition; Paper; Porous media; Characterization; Contact angle; Interfacial tension; Dynamic; Experimental tool; Wettability

Contact Information: a: Univ. Grenoble Alpes, CNRS, G-SCOP, 38000 Grenoble, France; b: Centre of Papermaking and Printing, Lodz University of Technology, 93-005 Lodz, Poland; c: BeFC SAS, 31 rue Gustave Eiffel, 38000 Grenoble, France & Soils, Solids, Structures, Risks Laboratory (3SR), University Grenoble-Alpes, 1270, rue de la piscine, 38610 Gières, France; d: BeFC SAS, 31 rue Gustave Eiffel, 38000 Grenoble, France; Corresponding author: pierre-yves.bloch@grenoble-inp.fr

INTRODUCTION

The interaction of liquids with porous materials is becoming more and more important as the number of applications of this phenomenon in new areas of technology increases. The vast majority of scientific interests focus on biological applications, such as blood tests, cosmetics (Attinger *et al*. 2013; Ahmed *et al*. 2017), DNA analysis, or drug delivery (Trybala *et al*. 2019). Liquid absorption and wetting dynamics are also important performance properties in high-speed printing (Rosenholm 2015; Krainer and Hirn 2018) and are the basis of microfluidic paper-based devices (µPADs) operation (Whitesides 2006; Garnier and Then 2013; Naseri *et al*. 2020). Indeed, there is a growing market trend to adopt µPADs that interact with fluids (*e.g*., forensic specimen collection, and filtration products). A myriad of fluids (*e.g.*, blood, sweat, saliva, river water, oil, *etc*.) and substrates

may be considered for such applications (Connelly *et al*. 2015). Another of µPADs key application is Lateral Flow Assays (LFAs), as these devices use a microfluidic paper strip in order to provide a simple and low-cost diagnostic for various medical applications (Oyola-Reynoso *et al*. 2015). LFAs are a major cornerstone for HIV, α-amylase (Dutta *et al*. 2016), malaria detection (Reboud *et al*. 2018), coagulation monitoring (Hegener *et al*. 2017), or hepatitis B virus testing. More recently, as a general trend toward patient-centric and delocalized healthcare, the approach has been demonstrated in the response to the COVID-19 pandemic *via* low-cost home testing kits. However, as LFAs have evolved to provide increased sensitivity and selectivity of *via* the use of exotic enhancers (*e.g*., fluorescent biomarkers (Sanjay *et al*. 2015)), there is a good argument for revisiting the porous media used to provide the assay. An effective industrially compatible characterization could therefore be of great value in this context. To design and optimize such devices, experimental characterization tools should be either used, or developed. One current research direction is the experimental investigation of the properties of porous substrates in order to provide further guidance in the selection of materials and/or fluids for specific applications. Today, the classical approach to estimating physical properties of the diffusion phenomenon exhibited by porous media has been either through calculation (Fries and Dreyer 2008; Ashari *et al*. 2010; Rosenholm 2015), or complex experimental equipment to characterize the structure such as microtomography or even x-rays synchrotron microtomography (Du Roscoat *et al*. 2005a). The objective of this paper is to demonstrate the possibility to both characterize the liquid imbibition properties through paper, and to conversely predict structural paper properties when the liquid properties are already known. Fibrous materials - specifically paper - are interesting to study due to the complexity of the phenomena that occur during their interaction with liquids. As a result, many research centers conduct research on the phenomena such as capillarity, diffusion, and spontaneous imbibition. Therefore, investigations related to paper materials in terms of their behavior during contact with liquid are of great practical importance.

Various alternative methods exist for investigating and identifying these physical phenomena and calculating empirical or physical parameters. Among these different approaches, both indirect and direct experimental devices can be distinguished. An indirect method consists of measuring a consequence of the studied phenomena, and not the phenomena itself (Du Roscoat *et al*. 2005b). The primary benefit of indirect technique lies in the in-situ precision attained, counterbalanced by drawbacks including the high cost associated with visualization, typical incompatibility with ultra-fast phenomena, and the potential generation of artifacts during the process of concatenation of 2D images into a 3D reconstruction, especially in the case of structural characterization at the micron size.

As a result, this method is very difficult to fully automate. The standard tests such as, for example, Cobb, Klemm, Hercules, Penetration Dynamics Analyzer (PDA), or Bristow (Ovaska and Backfolk 2018) exist for characterizing the imbibition of paper materials. The eXtended Liquid Penetration Analyzer, XLPA is introduced as a complementary experimental characterization. All these methods have advantages and limitations that are detailed in Table 1. The differences between the experimental devices are shown in Fig. 1.

To describe the XLPA equipment, its working principle, associated with an example of results, is presented in Fig. 2. Figure 2 shows the working device of the XLPA equipment, based on visual measurements of spontaneous imbibition and diffusion of liquids into porous materials (Olejnik *et al*. 2018).

Dynamic behaviour is revealed, allowing further analysis in terms of the morphology of the obtained ellipse shape. Regarding the bulging shape of the fluid above the nominal top of the reservoir, as the impact is currently unknown, it was decided to fill the reservoir with the same volume each time, hence leading in a similar shape for every test performed. The bulging shape of the meniscus would have more impact on significantly high-viscosity liquids.

Table 1. Experimental Methods to Characterize Fluid Imbibition into Paper Substrates: Pros and Cons

Method (Fig.1)	**Pros**	**Cons**
Cobb (i) *ISO 535:2023*	• Simple and widely used • Large data base with many paper references • Low-cost and low-complexity technology • Information on the amount of liquid absorption per surface area at longer time scales (*i.e.*, mins)	• Limited duration (minutes); cannot characterize phenomena at short time frames (ms) • Range of papers that are compatible with such test, no through flow (piercing) is allowed defined as a visual apparition of the considered fluid on the opposite side • Impossible to study anisotropy or two sidedness effect (non-symmetry in the thickness direction)
Klemm (ii) *ISO 8787:1986*	• Simple and widely used • Low-cost and low-complexity technology • Simultaneous comparison between different papers is possible • Possibility to distinguish “Machine-” and “Cross-” directions • Anisotropy can be studied	• No direct calculation • A classical criterion is set as the time required to reach a given vertical distance • Limited duration (minutes) • Impossible to characterize two sidedness effect
PDA (iii)	• Information about the speed of penetration • Short time scales possible (ms) • Possibility to study different fluids	• Equipment is not yet widely introduced in industry • Not yet a widely adopted as a standard • No volume of fluid penetration is obtained • Impossible to study anisotropy or two sidedness effect • Difficulties in quantitative comparison of different types of papers: the ultrasound beam power may significantly differ depending on the type of tested paper
Bristow (iv)	• Measurement of standardized ink absorbency • Represent the dynamic of fluid deposition of a fluid as the paper is moving (at different speeds, fixed by the rotation speed of the row) • Mimic coating unit operation	• Time-consuming method as few tests with different velocities of the wheel are required. Not a single test to obtain the characterization • Possible to study anisotropy or two sidedness effect
Hercules (v)	• Simple • This optical method is based on	• Long time scales only (s to min) • Represent the printing process of ink

TAPPI T530	standard ink penetration • Possible to study anisotropy or two sidedness effect	deposition • Equipment setup can be complex • Only a relative value is obtained as the results depend on the color of paper as the initial reflectance is considered
XLPA (vi)	• Rapid phenomenon observation (ms) • Automated method • The wetted area, knowing the thickness of the studied substrate leads to the volume of the fluid. Therefore, it is possible to determine the fluid inside the substrate • Possibility to extend the analysis of the data to obtain further physical parameters of either the fluids or the substrate (see below) • Possible to study anisotropy or two sidedness effect	• Post data treatment required • Not yet commercially available

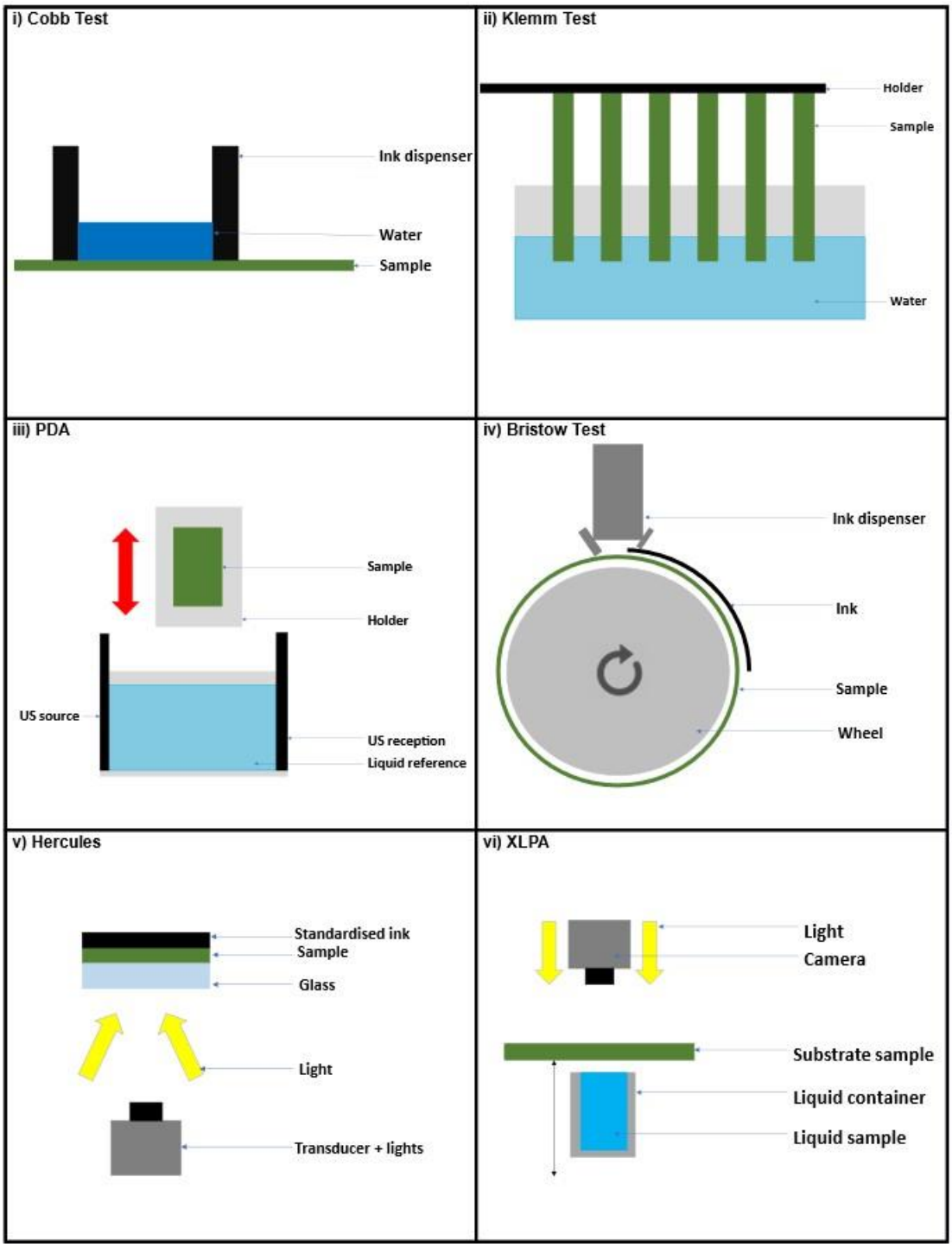

Fig. 1. Schematic representation of the different methods for characterization fluid imbibition (sizes not at scale) with i) Cobb test, ii) Klemm test, iii) Penetration Dynamic Analyzer (PDA), iv) Bristow test, v) Hercules tests and vi) EXtended Liquid Penetration Analyzer (XLPA). Standards are provided in Table 1.

The aim of the current work was to present a new attempt regarding the analysis of fluid flow and absorption dynamics phenomena in porous media using data obtained from the XLPA device.

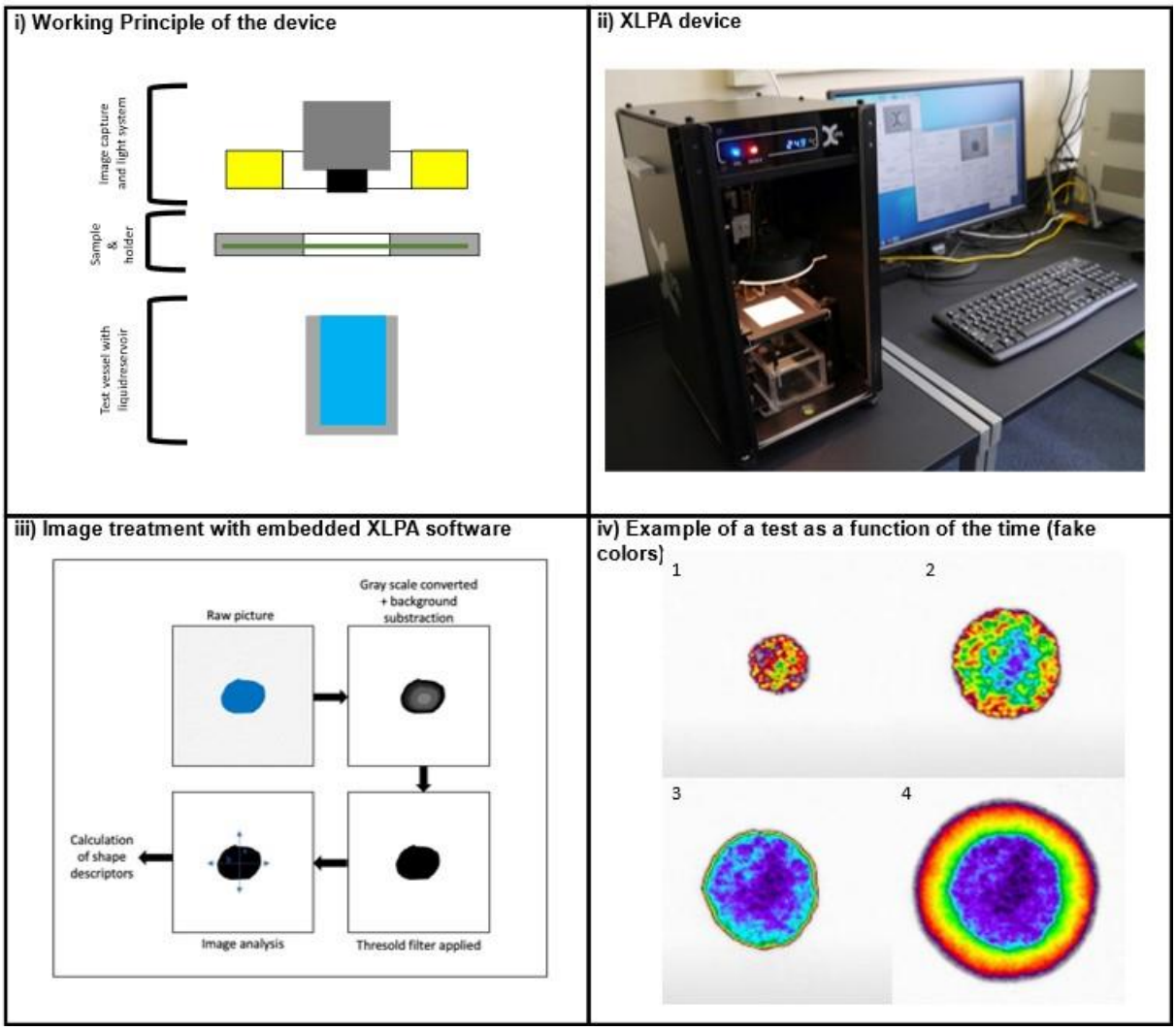

Fig. 2. XLPA device operation

EXPERIMENTAL

Materials

Two categories of tissue papers (commercial) were selected to conduct the experimental tests. Both were issued from the paper machine directly. The first category, identified as *Tissue 1*, is a toilet tissue, single layer, creped, single ply, taken directly from the paper machine. The thickness is 93 µm, and the basis weight was 18 $g.m^{-2}$. The second category, identified as *Tissue 2*, is a towel tissue, single layer, creped, single ply, taken directly from the paper machine. The thickness is 101 µm with a basis weight of 19 $g.m^{-2}$. The pulp composition for both *Tissue 1* and *Tissue 2* is 80% hardwood (eucalyptus), 12% softwood (pine), 4.5% of chemi-thermomechanical pulp (birch), and 3.5% broke pulp. Such materials are interesting for characterization, as they are more heterogeneous than blotter papers as well as developed for improved impregnation. The fluid used was DI water from MiliQ Direct-Q5.

The sample conditioning and storage influence the experimental results. If the standard conditioning (T = 23 ± 1 °C and 50±2% RH) is not available, the experimental environmental conditions are specified.

Theoretical Considerations

As the evolution of the fluid inside the porous materials is not linear *vs.* time, different time scales must be introduced for more precise process characterization. Moreover, an appropriate model must be selected for each time scale that will allow for a sufficiently accurate description of the studied phenomenon.

The first idea during the presented research, was to distinguish short and long-time evolutions. The initial linear model, referred as Quere (Quéré 1997), may find two geneses. According to the theoretical arguments presented by Quere, any model, even a non-linear one, can be assumed to be linear as a first approximation. For the purpose of the presented study, the Quere model will be referred to as the purely inertial model. The parameters *A* and *B* used in the model, are defined below.

Purely inertial model: Quere model

$$h = t\sqrt{B} \tag{1}$$

In Eq. 1, *h* and *s* represent the column height (mm) and the time (s), respectively. *B* is the model parameter. The time derivative may then be calculated:

$$\frac{\mathrm{d}h}{\mathrm{d}t} = \sqrt{B} \tag{2}$$

To understand the significance of the parameter *B*, the momentum balance of a liquid inside a capillary tube may be considered. The capillary pressure is balanced by the inertial forces, the viscous forces, and the hydrostatic pressure (Eq. 3), (Bosanquet 1923),

$$\frac{2\sigma cos\theta}{R} = \frac{d\left(\rho h\frac{\mathrm{d}h}{\mathrm{d}t}\right)}{dt} + \frac{8\mu h\frac{\mathrm{d}h}{\mathrm{d}t}}{R^2} + \rho g h \tag{3}$$

where σ, R, μ, θ, ρ, and γ, represent the surface tension (Nm^{-1}), the inner radius (m), the fluid viscosity (Pas), the contact angle (°), the fluid density (kgm^{-3}), and the interfacial tension (Nm^{-1}), respectively.

The parameters *A* and *B* are defined as follows:

$$A = \frac{8\mu}{R^2\rho} \tag{4}$$

$$B = \frac{2\sigma\cos\theta}{R\rho} \tag{5}$$

Then, neglecting both the gravity and the viscous terms and dividing by ρ, Eq. 3 leads to:

$$\frac{2\sigma\, cos\theta}{\rho R} = \frac{\partial\left(h\frac{\mathrm{d}h}{\mathrm{d}t}\right)}{\partial t} = \left(\frac{\mathrm{d}h}{\mathrm{d}t}\right)^2 + h\left(\frac{\mathrm{d}^2h}{\mathrm{d}t^2}\right) \tag{6}$$

Quere (1997) solved Eq. 6 by integration:

$$h = t\sqrt{\frac{2\sigma\cos\theta}{\rho R}} \tag{7}$$

Equation 7 predicts that the capillary rise, *h*, will be proportional to time. Note that as every non-linear model can be approximated with a 1st order linear model, this model may always be considered in the context of linear dependances. In addition, the transition between linear and non-linear can also be used as a way to refine understanding of the physical phenomenon at stake. With this model, *B* identification is straightforward. As the imbibition is not linear, the validity domain is reduced to short-term studies (seconds).

The long-time model is extracted from literature and is based on the most classical used model, the Lucas-Washburn model. This is also referred as the purely viscous model. Equation 8 refers to the proposed model (Lucas 1918; Washburn 1921; Zhmud *et al.* 2000),

$$h^2 = \frac{2B}{A}t \tag{8}$$

where *A* and *B* are defined in Eqs. 4 and 5. By calculating the square root, one obtains:

$$h = \sqrt{\frac{2B}{A}}\sqrt{t} = \sqrt{\frac{2Bt}{A}} \tag{9}$$

Using the fundamental principle of dynamics, Eq. 3, neglecting the inertial forces and the hydrostatic pressure, one obtains,

$$\frac{2\sigma\cos\theta}{R} = \frac{8\mu}{R^2}\,h\frac{\mathrm{d}h}{\mathrm{d}t} \tag{10}$$

which is equivalent to,

$$h\frac{\mathrm{d}h}{\mathrm{d}t} = \frac{\sigma R\cos\theta}{4\mu} \tag{11}$$

which implies by integration with $h(t{=}0) = 0$:

$$h^2 = t\,\frac{\sigma R\cos\theta}{2\mu} = \frac{2B}{A}t \tag{12}$$

This widely used model predicts a squared of height of capillary rise *vs.* time. Note that it is not considered from the initial time but as the regime for longer times (seconds to minutes). Thus, this model is usually used to represent a long-time scale (Hamraoui and Nylander 2002).

A third model is then introduced to consider the whole range of time. Obviously, this model, referred as the Bosanquet (1923), is less accurate when applied to short and long durations.

Visco-inertial mode: Bosanquet model

Based on the previous equations with the hypothesis of no gravity applied, using the fundamental principle of dynamics, Eq. 13 is proposed:

$$\frac{d}{dt}\left(h - \frac{\mathrm{d}h}{\mathrm{d}t}\right) + \left(A\,h\frac{\mathrm{d}h}{\mathrm{d}t}\right) = B \tag{13}$$

By integration this becomes:

$$h^2 = \frac{2B}{A}\left[t - \frac{1}{A}\,(1 - e^{-At})\right] \tag{14}$$

Then

$$h^2(t \to t_\infty) = \frac{2B}{A}\left(t - \frac{1}{A}\right) = \frac{2B}{A}\left[t - \frac{1}{A}(1 - e^{-At})\right] \tag{15}$$

which implies:

$$h^2 = \frac{2B}{A}\left[t - \frac{1}{A}(1 - e^{-At})\right] \quad (16)$$

$$h \approx \sqrt{\frac{2B}{A}\left[t - \frac{1}{A}(1 - e^{-At})\right]} \quad (17)$$

The Bosanquet model is highly non-linear. The model includes both inertial and viscous contributions, as it is based on the transition phase. While it is significantly more difficult to use, the Bosanquet model is taking both the Quere and Lucas-Washburn models into consideration (Fries and Dreyer 2008). A representation of these models is provided in Fig. 3.

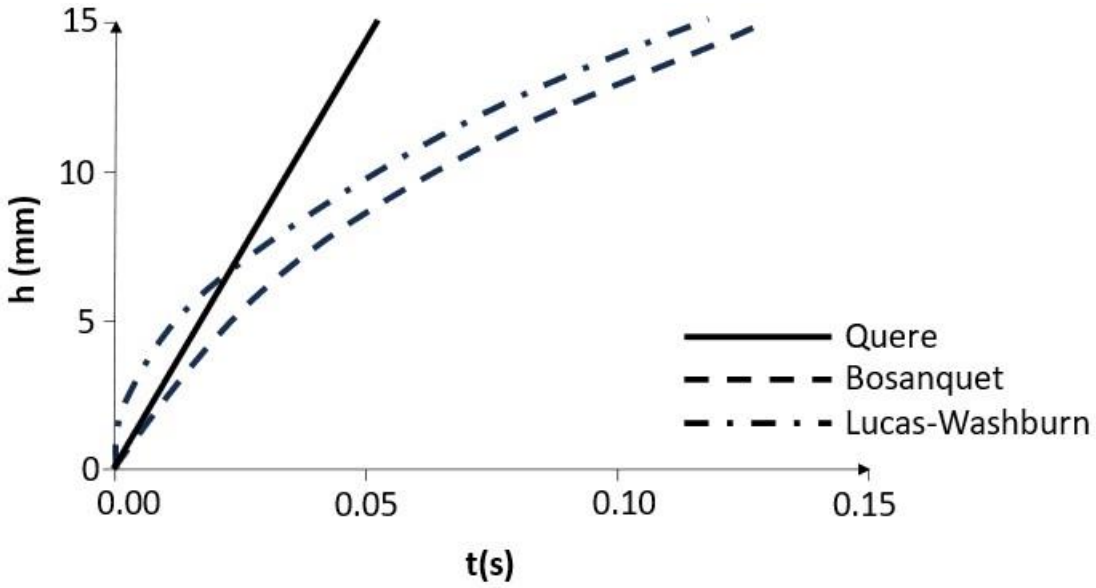

Fig. 3. Examples of models for purely inertial therefore proportional to time (Quere, Equation 1), purely viscous therefore proportional to square-root of time (Lucas-Washburn, Equation 9) or visco-inertial (Bosanquet, Equation 17)

The Bosanquet equation presented in Equation 17 converges into the Lucas-Washburn model to within one constant.

Parameter Definitions

Experimentations make it possible to identify the parameters (*A*, *B*) of the different models considered here. These parameters depend on physical quantities such as fluid viscosity, contact angle or pore diameter as presented in Eqs. 4 and 5.

In addition, the transition between linear and non-linear can also be used to better understand the described physical phenomenon. With this model, *B* identification is straight forward. As the imbibition is not linear, the validity domain is reduced to short-term studies (s).

Based on the identification of the model parameters, physical quantities, which are difficult to obtain experimentally, may be calculated. For example, the contact angle is traditionally measured on the material surface, but it is more difficult to measure it inside of the material's structure (bulk). Advanced technologies such as microtomography are necessary for such studies. As described in the previous equation, the contact angle depends

on the physico-chemistry, topography, and roughness (of the porous media or fibers). This has been also mentioned by Hubbe *et al*. (2015).

As *A* and *B* depend on cos(θ), *R* and γ for a given known or fixed material, *R*, cos(θ), and γ can be determined if needed. In addition, for fluids of known viscosity and surface tension, an effective pore radius characterizing the porous medium (*R*) may be determined.

RESULTS AND DISCUSSION

As the materials used are not isotropic, the obtained shape is often an ellipse, which may be characterized by its half-axis, *a* and *b* (please take into account that the letters *a* and *b* describe different parameters than *A* and *B*). An isotropic case corresponds to a circle, where *a* is equal to *b*. The greater the anisotropy is, the higher the ratio $\frac{a}{b}$ is, as illustrated in Fig. 4i.

The evolution of both the major and minor axis are also presented in Fig. 4. The anisotropy, which may be characterized by the anisotropy $\frac{a}{b}$ increases with time, as expected.

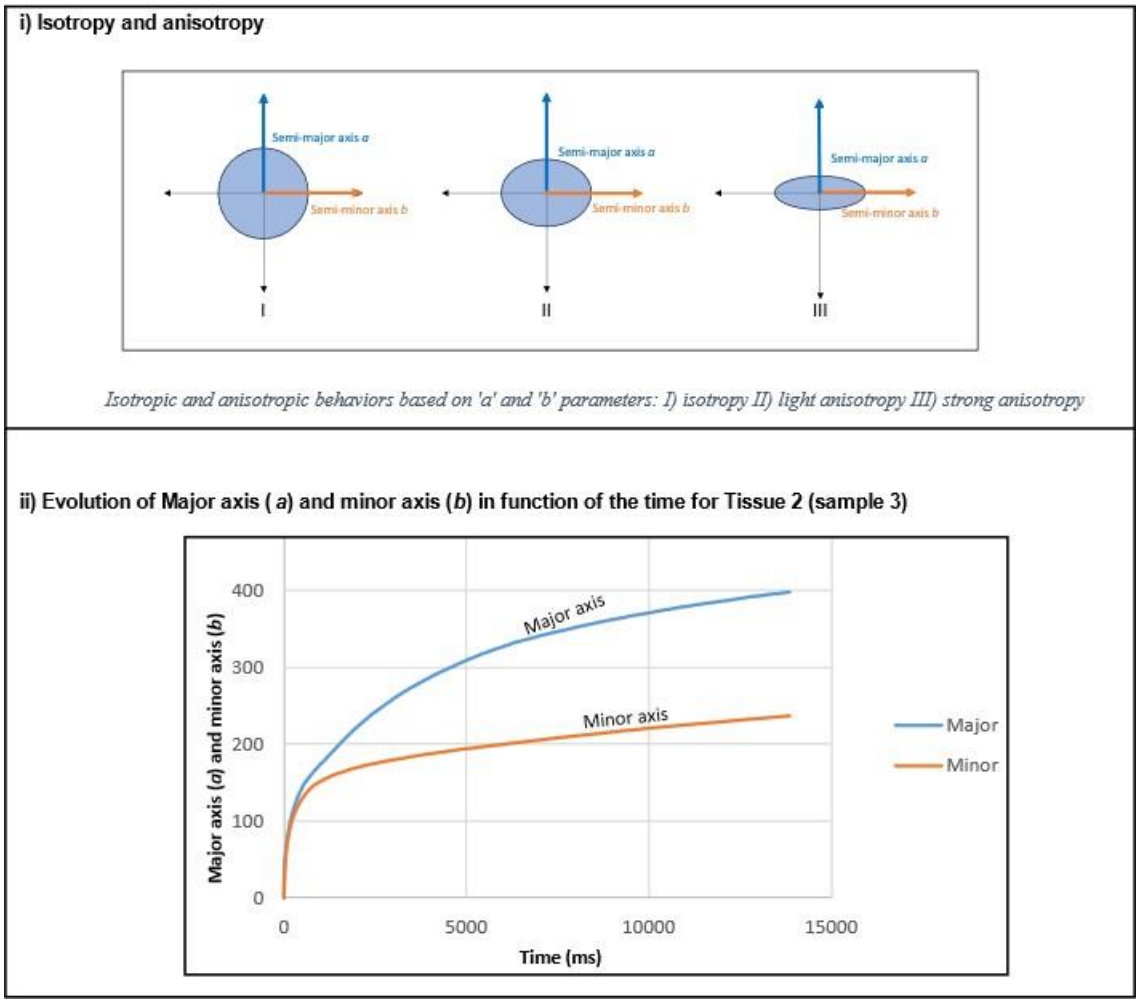

Fig. 4. i) Illustration of different anisotropic and isotropic behaviors and ii) Major(a) and minor(b) comparison for the same sample

Considering now the selected papers (toilet tissue designated as Tissue 1 and towel tissue designated as Tissue 2), measurements were conducted on 8 different samples from the same paper under the same exact conditions. Hence, the experimental results carried out on the 8 different samples (curves 1 to 8) are presented in Fig. 5, showing satisfactory repeatability.

The kinetics for Tissue 1 were higher than for Tissue 2. Indeed, Tissue 2 contained a hydrophobic agent and had a different crepe. As a result, its absorbency was higher than Tissue 1.

The relative variation for Tissue 1, Δ_1, was estimated at time = 140000 milliseconds:

$$\Delta_1\% = \frac{150}{1200} = 11.5\% \quad (18)$$

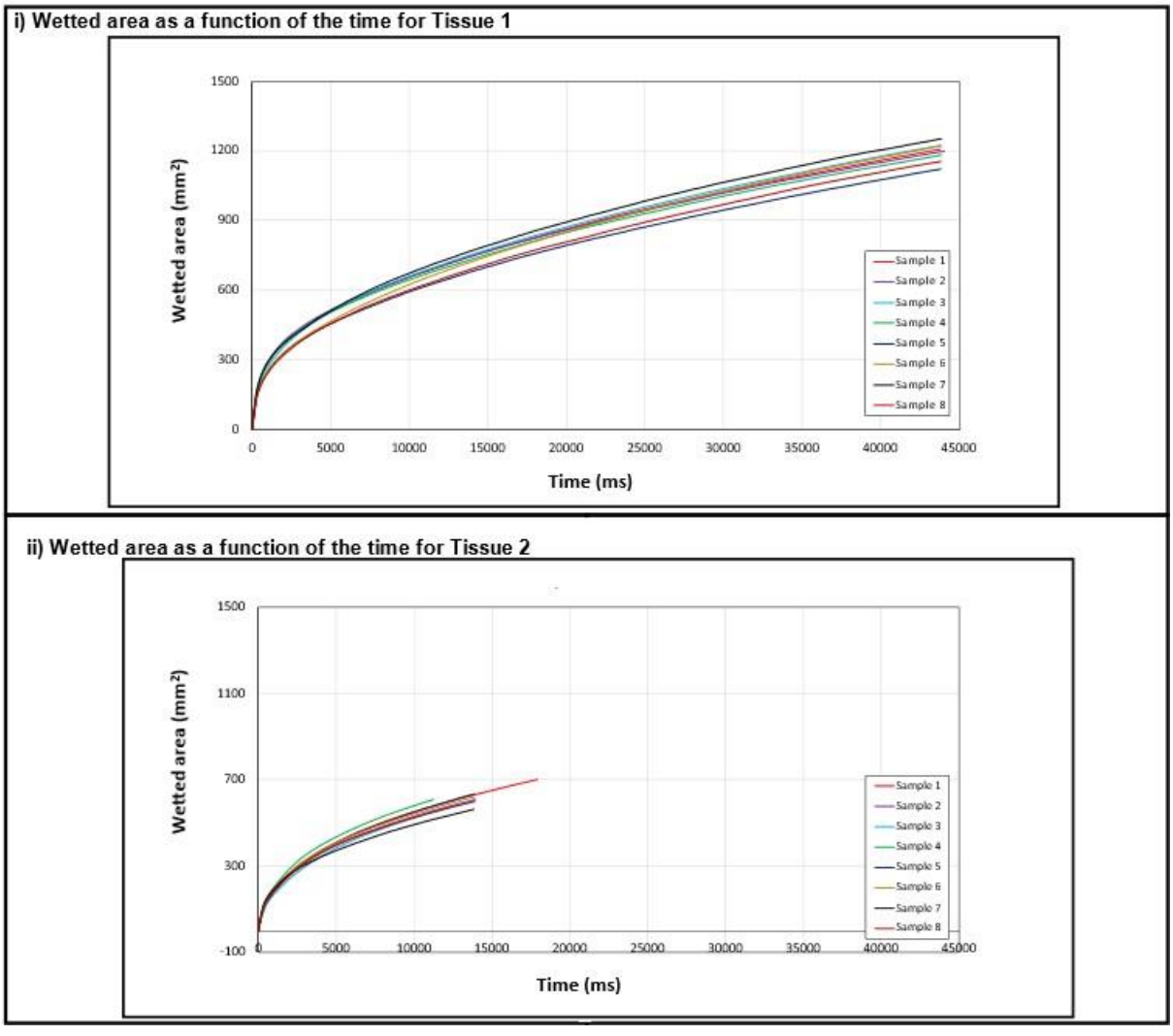

Fig. 5. Wetted area as a function of the time for Tissue 1 and Tissue 2

Similarly, the relative variation for Tissue 2, Δ_2, at time=14000 milliseconds:

$$\Delta_2 = \frac{50}{600} = 8.3\% \quad (19)$$

For Tissue 2 sample:

A single curve is considered as an illustration for Tissue 2 papers. A linear relationship between the main axis and time is first shown for short time. A linear relationship was considered between the square of the main axis versus time, for the long duration.

Thus, both models (Quere and Lucas-Washburn) were found to describe the experimental data in an acceptable way. In order to study the evolution of the major axis, both its value and its squared value were plotted as a function of time (Fig. 6).

For the mathematical fitting, a linear model was fitted. If a quantitative characterization is required, the model parameters can be calculated. Thus, the obtained results concerning the coefficient for curve presented in Fig. 6 i) leads to:

$$Leading\ coefficient = 0.2159 \approx \sqrt{b} \quad (20)$$

$$b = 0.0466 \quad (21)$$

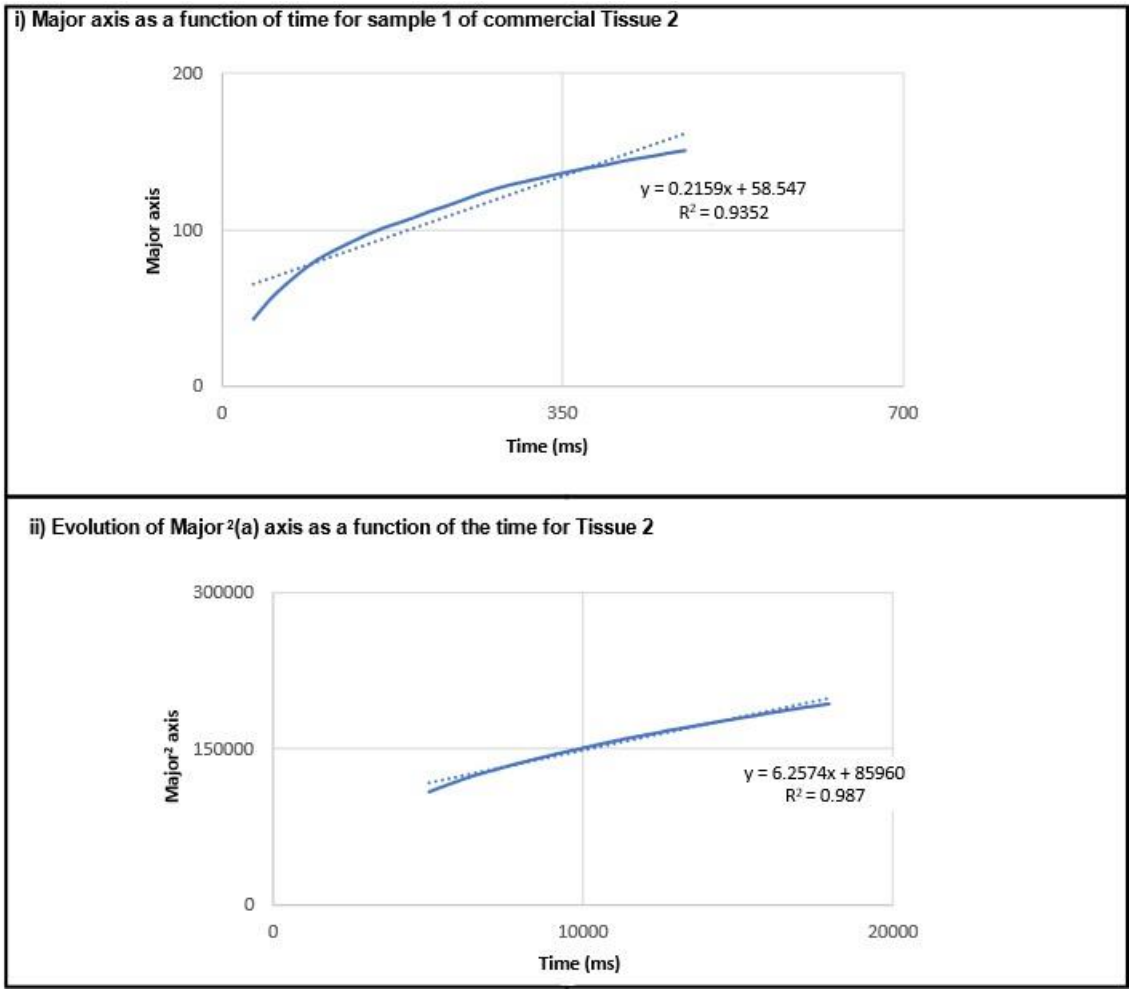

Fig. 6. Commercial Tissue 2 Major i) and Major^2 ii) as a function of the time

It follows that the leading coefficient for curve presented in Fig. 6 ii) can be estimated as:

$$Leading\ coefficient = 6.2574 \approx \frac{2b}{a} \quad (22)$$

$$a = \frac{2b}{6.2574} = 0.0149 \quad (23)$$

Introducing *a* and *b* in the equations leads to:

$$a = \frac{8\mu}{R^2\rho} <=> R = +\sqrt{\frac{8\mu}{a\rho}} \quad (24)$$

Numerical application:

For DI water, the following values were used: ρ=997 kgm^{-3} and μ= 10^{-3} Pas

$$R_{tissue2} = 0.0232 \text{ mm} = 23.2 \text{ µm} \quad (25)$$

Therefore, a characteristic size of pore of the structure: $R_{tissue2}$ = 23 µm may be obtained from the experimental tool.

For Tissue 1 sample:

A single curve is considered as an illustration for the Tissue 1 papers. Considering the tissue sample, the same methodology was used to analyse the obtained experimental data. First a linear relationship is presented for both the short and long time, for the main axis and its square value, respectively, as presented in Fig. 7.

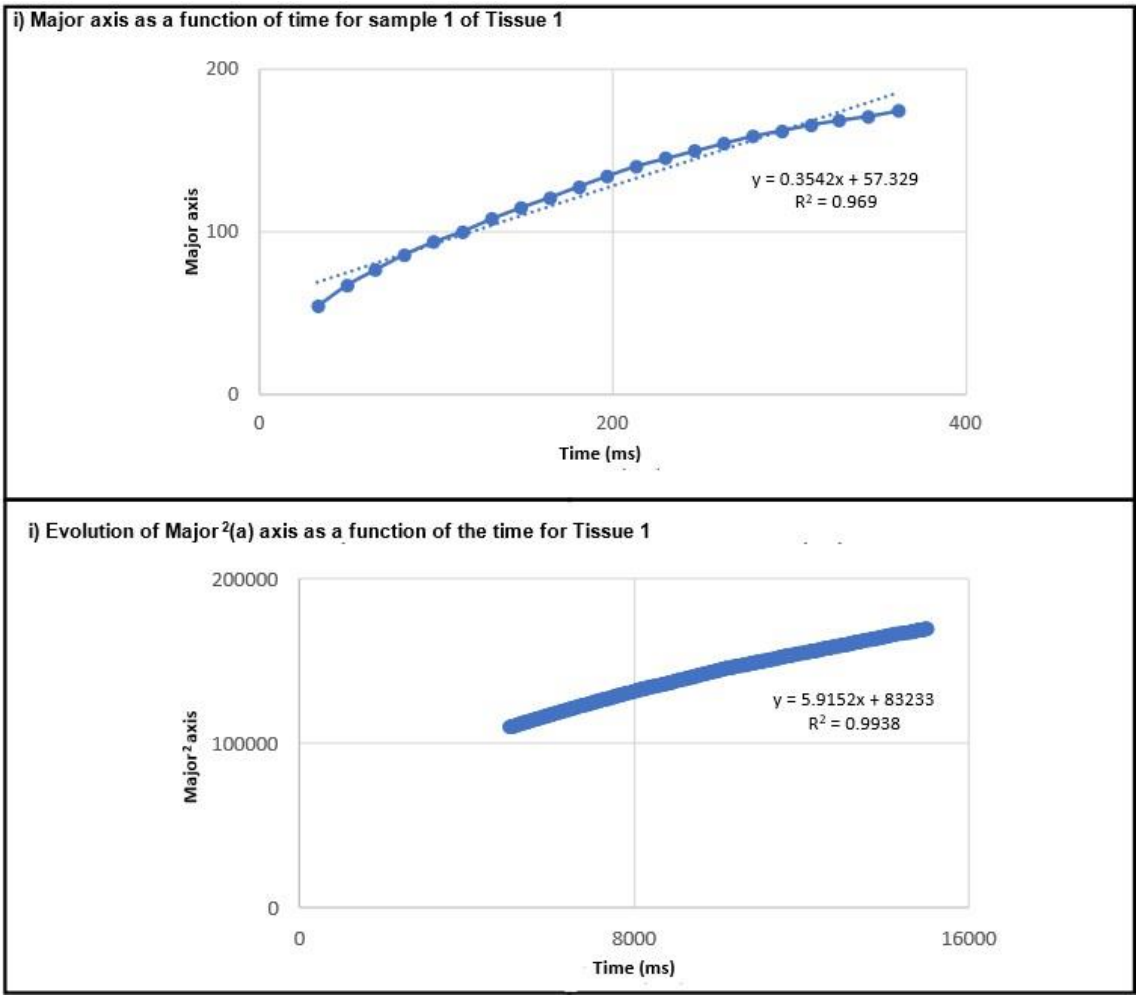

Fig. 7. Commercial Tissue 1 Major i) and Major^2 ii) as a function of the time

For the mathematical fitting, a linear model has been fitted. The leading coefficients may be obtained in Figs. 7 i) and 7 ii) as,

$$Leading\ coefficient = 0.3542 \approx \sqrt{b} \quad (26)$$

$$b = 0.1254 \quad (27)$$

Leading coefficient for curve 7ii:

$$Leading\ coefficient = 5.9152 \approx \frac{2b}{a} \quad (28)$$

$$a = \frac{2b}{5.9152} = 0.0424 \quad (29)$$

For DI water, given the following values can be applied, ρ=997 kgm^{-3} and μ= 10^{-3} Pas, leading to the following value of R:

$$R_{tissue1} = 0.0137 \text{ mm} = 14 \text{ µm} \quad (30)$$

Repeatability

To assess the repeatability, 8 samples were tested for each category. By calculating *a* and *b*, the coefficients of variations were determined (Table 2). By calculating the coefficient of variation from the thickness available in appendix, the ratio of those coefficients is found to be similar to the ratio of the coefficients of variations of model parameters. The hypothesis is that the variation in the measurement presumably comes from the local variations of the structure.

Table 2. Model Parameters (*a,b*) for Both Tissues in Order to Establish Both Averages and Coefficients of Variation

Sample #	Tissue 1		Tissue 2	
	Semi-major axis (a)	*Semi-minor axis (b)*	*Semi-major axis (a)*	*Semi-minor axis (b)*
1	0.0026	0.0993	0.0021	0.0491
2	0.0022	0.0832	0.0023	0.0529
3	0.0033	0.1222	0.0023	0.0455
4	0.0032	0.1266	0.0021	0.0481
5	0.0039	0.1471	0.0026	0.0621
6	0.0048	0.1956	0.0018	0.0398
7	0.0038	0.0990	0.0022	0.0553
8	0.0040	0.1219	0.0025	0.0562
Average	0.0035	0.1244	0.0023	0.0511
Coeff var	24.35	28.15	11.18	13.61

Example of applications

In this application, a paper with two different levels of calendering was considered. Calendering is a process of smoothing and compressing a material (paper) during production by passing a single continuous sheet through several pairs of rolls.

Whatman Grade 1, supplier = Cytiva. Thickness = 0.180 mm and Basis Weight = 87 $g.m^{-2}$. Level 1 of calendering is a linear charge of 20 $kg.cm^{-1}$, and level 2 is a linear charge of 40 $kg.cm^{-1}$. Regarding the fluid used, it is DI Water from MiliQ Direct-Q 5 UV ZRQSVR5WW. Whatman grade 1 (calenderer level 1) and Whatman grade 1 (calendered level 2) were compared, as illustrated on Table 3. In this case, there were no significant differences due to calendering, considering the initial high porosity and isotropy of the considered paper.

This work demonstrates that it is possible to apply the presented mathematical model to predict the diffusion properties during the fluid flow through the porous paper structure. The implications of this research extend beyond the scientific realm, as it contributes to the fundamental knowledge underpinning fluid behavior in anisotropic material such as tissues or paper. As the scientific world moves forward, the integration of physical and/or chemical modifications to substrates promises to unravel even more layers of characterization, unlocking our ability to harness the potential of porous materials for technological breakthroughs.

Table 3. Comparison for a, b, and R for Whatman Grade 1 and DI Water for Level 1 and 2 of Calendering

Parameters for Whatman Grade 1 and DI Water	Calendered level 1	Calendered level 2
a	0.0009759	0.0009623
b	0.01331	0.01280
R (mm)	0.0906	0.09130

To go further in the analysis, plots were made showing the evolution of both semi-major axis and semi-minor axis versus time, squared root of the time and corrected initial time. An illustration of such results is introduced in Fig. 8.

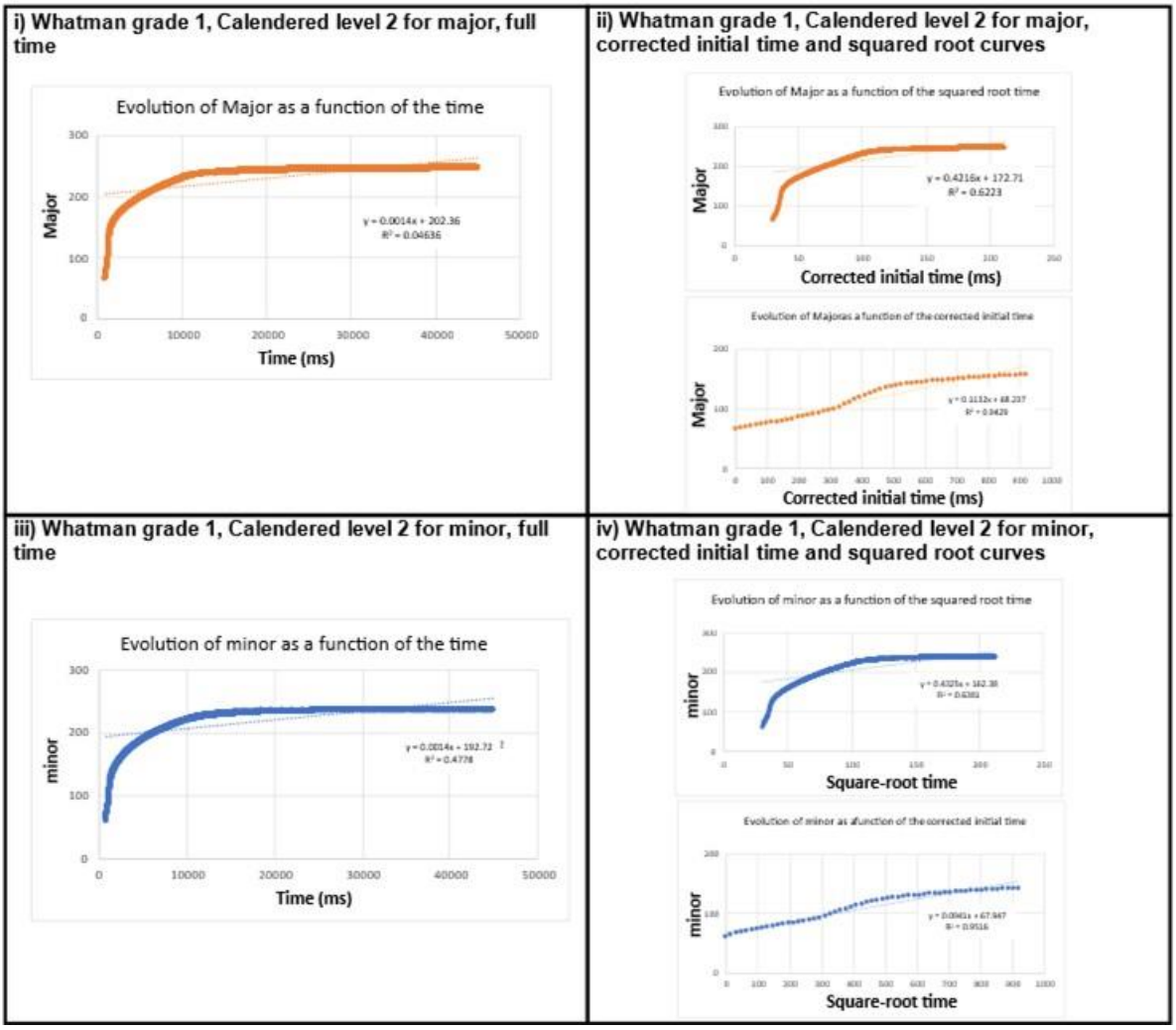

Fig. 8. Application example with Whatman Grade 1 calendered level 2 samples with i) semi-major axis in full time, ii) semi-major axis with corrected time and square-root of the time, iii) semi-minor axis in full time, ii) semi-minor axis with corrected time and square-root of the time

For the mathematical fitting, a linear model was chosen. It was observed that the Lucas-Washburn model did not match the measurements for the initial times. Accordingly, it was decided to neglect the capillary forces, which are expected to act in a horizontal direction. In addition, a potential force, ΔP_i, driven by the vertical movement of the test vessel was neglected, as all the tests were performed with the exact same conditions. Therefore, until ΔP_i is taken into consideration, the model is a 2D model. It was also decided to neglect all potential effects of thermal phenomena. The fluid is contained in a finite reservoir, leading to a boundary-limited regime. The considered imbibition is qualified as spontaneous.

CONCLUSIONS

A key accomplishment of this study lies in the ability to analyze flow and imbibition phenomena in porous media for short and long times. By shedding light on the intricate interplay between material, fluid behavior, and their inherent properties, progress has been

made towards enhancing a more efficient selection of raw materials in various applications ranging from industrial printing processes or medical devices. The challenges posed by different time scales can be addressed by selecting the most adequate experimental approach. The limitations of conventional methods have been transcended by this method using the eXtended Liquid Penetration Analyzer (XLPA).

The advantages of the work presented in this article is the possibility to study different time scales associated to a repeatable and quantitative experimental method. In addition, a way is provided to obtain physical properties, such as an effective radius R calculated for both tissues in Eqs. 25 and 30. Another benefit of the proposed approach is the opportunity to study short-time effects (milliseconds) while being quantitative. A suggested further experimentation is the characterisation of the impact of the anisotropy or the two-sidedness effect within the proposed approach.

The approach also offers the possibility to characterise different regimes. Some limitations need to be noted, however. The main one is the need for post-treatment analysis with specific skills. On the experimental method, three specific cases could be challenging. The first one is the test of a fluid that evaporates quickly, such as specific solvents or inks. Other challenging studies would be the characterisation of opaque materials or highly viscous fluids. The method described in this article, presenting a combined experimental and theoretical approach, could be used for paper or non-woven materials in various domains such as LFAs or printing process optimisation.

ACKNOWLEDGEMENTS

Mathieu PARVI and Arthur JANODET for their useful advice during the sample preparation and data treatment are gratefully acknowledged.

REFERENCES CITED

Ahmed, G., Arjmandi Tash, O., Cook, J., Trybala, A., and Starov, V. (2017). "Biological applications of kinetics of wetting and spreading," *Advances in Colloid and Interface Science* 249, 17-36. DOI: 10.1016/j.cis.2017.08.004

Ashari, A., Bucher, T. M., Tafreshi, H. V., Tahir, M. A., and Rahman, M. S. A. (2010). "Modeling fluid spread in thin fibrous sheets: Effects of fiber orientation," *International Journal of Heat and Mass Transfer* 53(9–10), 1750-1758. DOI: 10.1016/j.ijheatmasstransfer.2010.01.015

Attinger, D., Moore, C., Donaldson, A., Jafari, A., and Stone, H. A. (2013). "Fluid dynamics topics in bloodstain pattern analysis: Comparative review and research opportunities," *Forensic Science International* 231, 375-396. DOI: 10.1016/j.forsciint.2013.04.018

Bosanquet, C. H. (1923). "LV. On the flow of liquids into capillary tubes," *The London, Edinburgh, and Dublin Philosophical Magazine and Journal of Science,* Informa UK Limited, 45(267), 525-531. DOI: 10.1080/14786442308634144

Connelly, J. T., Rolland, J. P., and Whitesides, G. M. (2015). "'Paper machine' for molecular diagnostics," *Analytical Chemistry* 87(15), 7595-7601. DOI: 10.1021/acs.analchem.5b00411

Dutta, S., Mandal, N., and Bandyopadhyay, D. (2016). "Paper-based α-amylase detector for point-of-care diagnostics," *Biosensors and Bioelectronics,* 78, 447-453. DOI: 10.1016/j.bios.2015.11.075

Fries, N., and Dreyer, M. (2008a). "The transition from inertial to viscous flow in capillary rise," *Journal of Colloid and Interface Science* 327(1), 125-128. DOI: 10.1016/j.jcis.2008.08.018

Fries, N., and Dreyer, M. (2008b). "The transition from inertial to viscous flow in capillary rise," *Journal of Colloid and Interface Science* 327(1), 125-128. DOI: 10.1016/J.JCIS.2008.08.018

Garnier, G., and Then, W. L. (2013). "Paper microfluidics: Applications and perspectives," in: *Advances in Pulp and Paper Research, Trans. of the XVth Fundamental Research Symposium*, Cambridge, UK, 2013, S. J. I'Anson (ed.), pp. 541-583. DOI: 10.15376/frc.2013.2.541

Hamraoui, A., and Nylander, T. (2002). "Analytical approach for the Lucas-Washburn equation," *Journal of Colloid and Interface Science* 250(2), 415-421. DOI: 10.1006/jcis.2002.8288

Hegener, M. A., Li, H., Han, D., Steckl, A. J., and Pauletti, G. M. (2017). "Point-of-care coagulation monitoring: First clinical experience using a paper-based lateral flow diagnostic device," *Biomedical Microdevices* 19(3). DOI: 10.1007/s10544-017-0206-z

Hubbe, M. A., Gardner, D. J., and Shen, W. (2015). "Contact angles and wettability of cellulosic surfaces: A review of proposed mechanisms and test strategies," *BioResources* 10(4), 8657-8749. DOI: 10.15376/biores.10.4.Hubbe_Gardner_Shen

Krainer, S., and Ulrich, H. (2018). "Short timescale wetting and penetration on porous sheets measured with ultrasound, direct absorption and contact angle," *RSC Advances* 8(23), 12861-12869. DOI: 10.1039/c8ra01434e

Lucas, R. (1918). "Ueber das Zeitgesetz des kapillaren Aufstiegs von Flüssigkeiten," *Kolloid-Zeitschrift* 23, 15-22. DOI: 10.1007/BF01461107

Naseri, M., Simon, G. P., and Batchelor, W. (2020). "Development of a paper-based microfluidic system for a continuous high-flow-rate fluid manipulation," *Analytical Chemistry* 92(10), 7307–7316. DOI: 10.1021/acs.analchem.0c01003

Olejnik, K., Pełczyński, P., Bogucka, M., and Głowacka, A. (2018). "Optical measurement of the hydrophobic properties of paper products," *Measurement: Journal of the International Measurement Confederation* 115, 52-63. DOI: 10.1016/j.measurement.2017.10.020

Ovaska, S. S., and Backfolk, K. (2018). "The versatility of the Bristow absorption tester - A review," *Nordic Pulp and Paper Research Journal* 33(2). DOI: 10.1515/npprj-2018-3040

Oyola-Reynoso, S., Heim, A. P., Halbertsma-Black, J., Zhao, C., Tevis, I. D., Çinar, S., Cademartiri, R., Liu, X., Bloch, J. F., and Thuo, M. M. (2015). "Reprint of 'Draw your assay: Fabrication of low-cost paper-based diagnostic and multi-well test zones by drawing on a paper,'" *Talanta* 145, 73-77. DOI: 10.1016/j.talanta.2015.09.042

Quéré, D. (1997). "Inertial capillarity," *Europhys. Lett*. 39(5).

Reboud, J., Xu, G., Garrett, A., Adriko, M., Yang, Z., Tukahebwa, E. M., Rowell, C., and Cooper, J. M. (2018). "Paper-based microfluidics for DNA diagnostics of malaria in low resource underserved rural communities," *Enlighten Research Data.* DOI: 10.5525/gla.researchdata.722

Rolland Du Roscoat, S., Bloch, J. F., and Thibault, X. (2005a). "Synchrotron radiation microtomography applied to investigation of paper," *Journal of Physics D: Applied Physics* 38(10 A). DOI: 10.1088/0022-3727/38/10A/015

Rolland Du Roscoat, S., Bloch, J.-F., and Thibault, X. (2005b). "Characterisation of the 3D paper structure with X-ray synchrotron radiation microtomography," Trans. of the XIIIth Fund. Res. Symp. Cambridge, Manchester, 901-920. DOI: 10.15376/frc.2005.2.901

Rosenholm, J. B. (2015). "Liquid spreading on solid surfaces and penetration into porous matrices: Coated and uncoated papers," *Advances in Colloid and Interface Science* 220, 8-53. DOI: 10.1016/j.cis.2015.01.009

Sanjay, S. T., Fu, G., Dou, M., Xu, F., Liu, R., Qi, H., and Li, X. (2015). "Biomarker detection for disease diagnosis using cost-effective microfluidic platforms," *Analyst* 2015(21). DOI: 10.1039/c5an00780a

Trybala, A., Koursari, N., Johnson, P., Arjmandi-Tash, O., and Starov, V. (2019). "Interaction of liquid foams with porous substrates," *Current Opinion in Colloid and Interface Science* 39, 212-219. DOI: 10.1016/j.cocis.2019.01.011

Washburn, E. W. (1921). "The dynamics of capillary flow," *Physics Review* 17(3), 273-283. DOI: 10.1103/PhysRev.17.273

Whitesides, G. M. (2006). "The origins and the future of microfluidics," *Nature* 442, 368-373. DOI: 10.1038/nature05058

Zhmud, B. V., Tiberg, F., and Hallstensson, K. (2000). "Dynamics of capillary rise," *Journal of Colloid and Interface Science* 228(2), 263-269. DOI: 10.1006/jcis.2000.6951

Article submitted: October 5, 2023; Peer review completed: October 21, 2023; Revised version received: November 2, 2023; Accepted: November 3, 2023; Published: November 16, 2023.
DOI: 10.15376/biores.19.1.345-365

SUPPLEMENTAL INFORMATION

XLPA Configuration

Grey color algorithm = HSL with parameters:

GrayLevel= 0.299R + 0.587G + 0.114B

Background is subtracted.
Absolute threshold value = 200

Main Parameters of Image Analysis (Fiji®)

Program FiJi

- Step 1: Process, Median, Radius = 6
- Step 2: Set measurements: Area, Shape descriptors, Perimeter, Fit ellipse, decimal=3
- Step 3: Analyze particles: Display clear include summarize

Data Thickness Measurements Table in microns

Sample #	Tissue 1	Tissue 2
Sample 1	95	103
Sample 2	103	101
Sample 3	90	99
Sample 4	88	104
Sample 5	90	97
Sample 6	92	102
Sample 7	88	101
Sample 8	91	103
Sample 9	90	101
Sample 10	95	98
Sample 11	91	97
Sample 12	94	104
Sample 13	95	102
Sample 14	94	101
Sample 15	94	103
Average	92.7	101.1
Standard-Dev	3.8	2.3
Coeff variation	4.1	2.3

Repeatability Tests as a Function of the Squared Root of the Time